Heterozygous Deficiency of *PHD2* Restores Tumor Oxygenation and Inhibits Metastasis via Endothelial Normalization

Massimiliano Mazzone,[1,2,11] Daniela Dettori,[1,2,3,11] Rodrigo Leite de Oliveira,[1,2,11] Sonja Loges,[1,2] Thomas Schmidt,[1,2] Bart Jonckx,[1,2] Ya-Min Tian,[4] Anthony A. Lanahan,[5] Patrick Pollard,[4] Carmen Ruiz de Almodovar,[1,2] Frederik De Smet,[1,2] Stefan Vinckier,[1,2] Julián Aragonés,[1,2] Koen Debackere,[1,2] Aernout Luttun,[6] Sabine Wyns,[1,2] Benedicte Jordan,[7] Alberto Pisacane,[8] Bernard Gallez,[7] Maria Grazia Lampugnani,[9] Elisabetta Dejana,[9] Michael Simons,[5] Peter Ratcliffe,[4] Patrick Maxwell,[10] and Peter Carmeliet[1,2,*]

[1]Vesalius Research Center, VIB-Vlaams Instituut voor Biotechnologie, 3000 Leuven, Belgium
[2]Vesalius Research Center, Katholieke Universiteit Leuven, 3000 Leuven, Belgium
[3]Laboratory of Cancer Genetics, Institute for Cancer Research and Treatment, University of Turin Medical School, 10060 Candiolo, Turin, Italy
[4]The Henry Wellcome Building of Genomic Medicine, Oxford OX3 7BN, UK
[5]Cardiovascular Medicine, Yale University, New Haven, CT 06510, USA
[6]Center for Molecular and Vascular Biology, Katholieke Universiteit Leuven, 3000 Leuven, Belgium
[7]Biomedical Magnetic Resonance Unit, Medicinal Chemistry and Radiopharmacy U.C. Louvain, 1000 Brussels, Belgium
[8]Unit of Pathological Anatomy, Institute for Cancer Research and Treatment, 10060 Candiolo, Turin, Italy
[9]Vascular Biology Unit, Italian Foundation for Cancer Research Institute of Molecular Oncology, 20139 Milan, Italy
[10]Rayne Institute, University College London, London WC1E 6JJ, UK
[11]These authors contributed equally to this work
*Correspondence: peter.carmeliet@med.kuleuven.be
DOI 10.1016/j.cell.2009.01.020

SUMMARY

A key function of blood vessels, to supply oxygen, is impaired in tumors because of abnormalities in their endothelial lining. PHD proteins serve as oxygen sensors and may regulate oxygen delivery. We therefore studied the role of endothelial PHD2 in vessel shaping by implanting tumors in *PHD2*^{+/−} mice. Haplodeficiency of *PHD2* did not affect tumor vessel density or lumen size, but normalized the endothelial lining and vessel maturation. This resulted in improved tumor perfusion and oxygenation and inhibited tumor cell invasion, intravasation, and metastasis. Haplodeficiency of *PHD2* redirected the specification of endothelial tip cells to a more quiescent cell type, lacking filopodia and arrayed in a phalanx formation. This transition relied on HIF-driven upregulation of (soluble) VEGFR-1 and VE-cadherin. Thus, decreased activity of an oxygen sensor in hypoxic conditions prompts endothelial cells to readjust their shape and phenotype to restore oxygen supply. Inhibition of PHD2 may offer alternative therapeutic opportunities for anticancer therapy.

INTRODUCTION

Numerous studies have examined how blood vessels branch, but little is known about the morphogenesis of the endothelial cell (EC) layer. Nonetheless, a malshaped endothelium in "abnormalized" tumor vessels impairs perfusion and oxygenation (Jain, 2005). The resultant hypoxia promotes invasion, metastasis, and malignancy (Sullivan and Graham, 2007). Tumor hypoxia, together with hypoperfusion and increased interstitial pressure, impedes delivery and efficacy of anticancer drugs. Vessel normalization has therefore gained interest as a therapeutic option to improve drug delivery and anticancer treatment (Jain, 2005). Nonetheless, current antiangiogenic agents induce tumor hypoxia by pruning vessels or forming hypoperfused vessels, which can stimulate angiogenesis and limit their success (Bergers and Hanahan, 2008).

Endothelial "tip cells" at the forefront of a sprouting vessel navigate by extending filopodia; "stalk cells" trail behind and elongate the branch (Gerhardt et al., 2003). Both cell types have distinct molecular signatures. Much less is known about the EC type in nongrowing, quiescent vessels that maintain lumen patency and form a tightly aligned, orderly shaped EC layer with a cobblestone appearance.

Since supply of oxygen is an ancestral function of vessels, we hypothesized that vessels should have mechanisms to sense and adapt to changes in oxygen supply and, hence, perfusion in case of oxygen shortage. The oxygen-sensing prolyl hydroxylase domain proteins (PHD1–3) target hypoxia-inducible transcription factors (HIFs) for degradation (Kaelin and Ratcliffe, 2008). When oxygen tension drops, PHDs become less active, upon which stabilized HIFs mount an adaptive response, such as angiogenesis (Semenza, 2003). However, severe tumor hypoxia causes excessive release of angiogenic cytokines and, thereby, tumor vessel abnormalization (Jain, 2005).

The role of the oxygen sensors in angiogenesis has not been extensively studied. Inhibition of PHDs and silencing or
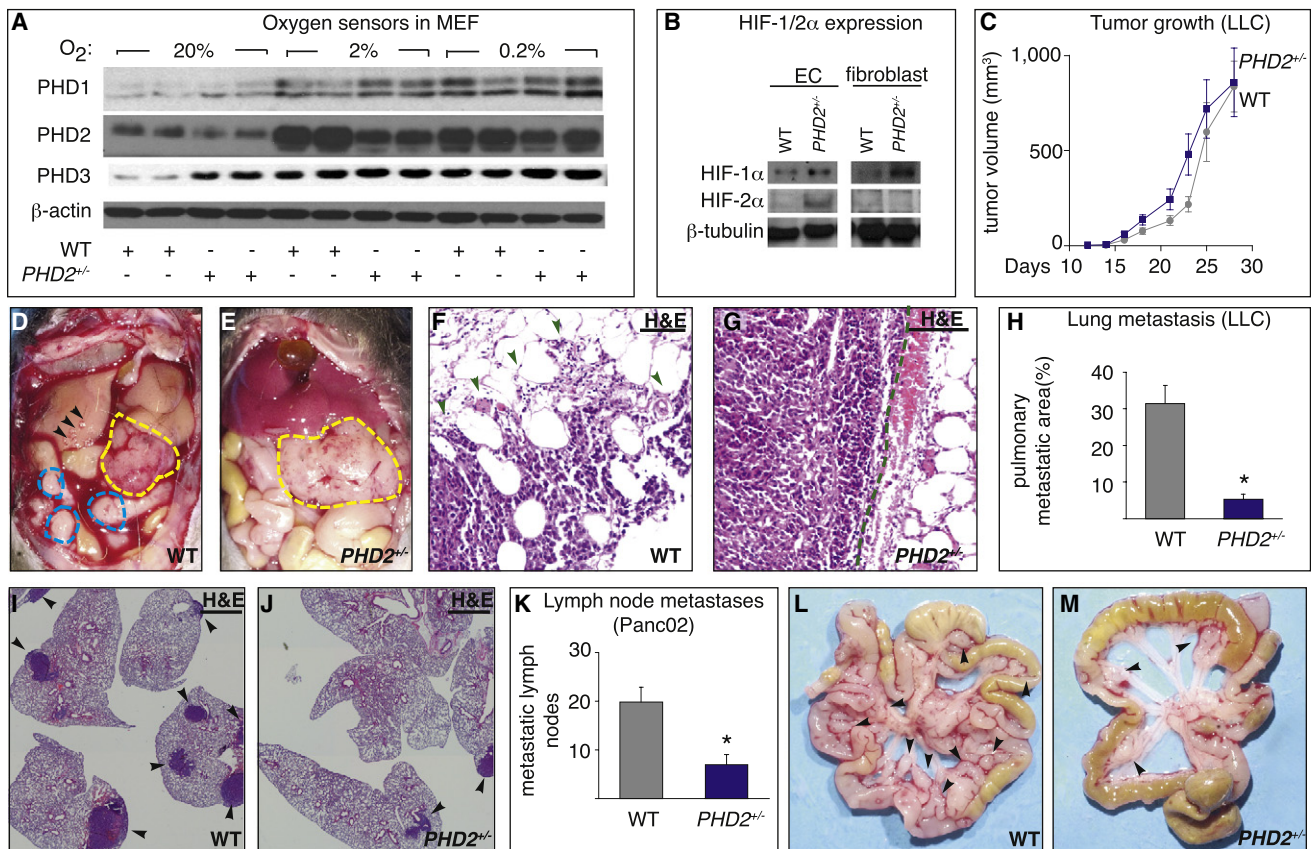
Figure 1. Reduced Tumor Invasion and Metastasis in $PHD2^{+/-}$ Mice
(A and B) Immunoblot of PHDs in mouse embryonic fibroblasts (MEF) (A) and of HIFs in endothelial cells (EC) and fibroblasts (MEF) (B).
(C) Growth of LLC tumors (n = 8; p = 0.33).
(D and E) Panc02 tumors (yellow line) are more invasive and metastatic in WT than $PHD2^{+/-}$ mice, as evidenced by hemorrhagic ascites, metastatic nodules (blue line), jaundiced liver, and liver metastases (arrowheads).
(F and G) Hematoxylin and eosin (H&E) staining showing infiltrative B16 tumor foci in WT mice ([F]; arrowheads) but encapsulated borders in $PHD2^{+/-}$ mice ([G]; dashed line).
(H) Reduced metastasis of LLC tumors in $PHD2^{+/-}$ mice (n = 8; p < 0.0001).
(I and J) H&E staining revealing fewer pulmonary metastatic LLC tumor nodules in $PHD2^{+/-}$ mice (arrowheads).
(K) Reduced metastasis of Panc02 tumor cells in $PHD2^{+/-}$ mice (n = 27; p = 0.0001).
(L and M) Macroscopic view showing more metastatic mesenteric lymph nodes (arrowheads) in WT (L) than $PHD2^{+/-}$ (M) mice.
Scale bars represent 50 μm in (F), (G), (I), and (J). Asterisks in (H) and (K) denote statistical significance. Error bars in (C), (H), and (K) show the standard error of the mean (SEM); all subsequent error bars are defined similarly.

inactivation of PHD2 after birth stimulate angiogenesis (Milkiewicz et al., 2004; Nangaku et al., 2007; Takeda et al., 2007; Wu et al., 2008), while overexpression of PHD2 in immortalized ECs suppresses proliferation via hydroxylation-independent mechanisms (Takeda and Fong, 2007). It is, however, unknown whether PHDs regulate EC morphogenesis, vessel normalization, or oxygen delivery. Here, we studied the role of PHD2 in these processes, using tumor vessel abnormalization as a model.

RESULTS

Generation of $PHD2^{+/-}$ Mice and Expression of PHD2
To study its biological role in vivo, we inactivated the *PHD2* gene (Figure S1A available online). PHD2-deficient ($PHD2^{-/-}$) mice died at midgestation, while $PHD2^{+/-}$ mice were healthy and displayed normal angiogenesis (Table S1, Figure S2). PHD2 was undetectable in $PHD2^{-/-}$ embryos (Figures S1B and S1C) and present at 50% of wild-type (WT) levels in $PHD2^{+/-}$ mice and cells at various oxygen tensions (Figure 1A and Figure S3A). As PHDs are HIF targets (Epstein et al., 2001; Marxsen et al., 2004), PHD3 and, to a lesser extent, PHD1 levels were upregulated in $PHD2^{+/-}$ conditions (Figure 1A and Figure S3A). PHD2 becomes gradually less active in hypoxia but still retains activity at low oxygen tensions (Epstein et al., 2001). HIF-1α levels were indeed higher in $PHD2^{+/-}$ cells at every, even low, oxygen tension (Figure 1B and Figure S3B); HIF-2α levels were also upregulated, particularly in ECs (Figure 1B). By resetting their oxygen-sensing curve, $PHD2^{+/-}$ cells act as if they continuously sense lower oxygen tensions, as if they are (pre)-adapted to hypoxia.

To study the role of stromal PHD2 in tumors without confounding effects of a role of PHD2 in malignant cells, we used chimeric tumor models, by implanting, in $PHD2^{+/-}$ mice, various $PHD2^{+/+}$ tumor cells: B16 melanoma, Panc02 pancreatic carcinoma, and Lewis lung carcinoma (LLC) cells. In vitro, PHD2 was detectable in all tumor lines, blood and lymphatic ECs, and fibroblasts (Figures S3C–S3E). In vivo, tumor, endothelial and fibroblast cells were PHD2 positive (Figures S3F–S3H). In $PHD2^{+/-}$ mice, transcript levels of PHD2 and PHD3 were reduced in tumors and ECs, freshly isolated from tumors, and immediately analyzed without subculturing (Figures S3I and S3J; see below for interpretation).

Tumors Grow Normally, but Metastasis Is Reduced in $PHD2^{+/-}$ Mice

Ectopic B16 and LLC tumors, or orthotopic Panc02 tumors, grew at a comparable rate in both genotypes (Figure 1C and Figure S4) and had comparable tumor cell proliferation and apoptosis (data not shown). Tumors in $PHD2^{+/-}$ mice appeared less "bloody" (Figures 1D and 1E). As HIFs promote metastasis, we expected that tumors in $PHD2^{+/-}$ mice would metastasize aggressively. However, in $PHD2^{+/-}$ mice, B16 tumors were encapsulated, grew focally, did not infiltrate surrounding tissues (Figures 1F and 1G), and metastasized less (percent of lung sections with metastases: 23% ± 3% in WT versus 7% ± 4% in $PHD2^{+/-}$; n = 6; p = 0.01). Also, LLC tumors grew noninvasively (data not shown), while pulmonary metastasis was reduced by 94% in $PHD2^{+/-}$ mice (Figures 1H–1J and Figures S5A–S5D). After resection of the primary tumor, haplodeficiency of $PHD2$ offered a survival benefit because of the reduced metastasis (Figure S5E).

Panc02 tumors in $PHD2^{+/-}$ mice grew as encapsulated tumors, while tumors in WT mice invaded the stomach and duodenum (Figures 1D and 1E). Histologically, 50% of WT but none of $PHD2^{+/-}$ mice had tumors with infiltrative margins (data not shown). Also, liver metastasis was reduced in $PHD2^{+/-}$ mice: 75% of WT mice but only 38% of $PHD2^{+/-}$ mice had hepatic nodules, with 3.5 ± 0.8 nodules per WT mouse, but only 0.7 ± 0.3 nodules per $PHD2^{+/-}$ mouse (n = 6; p = 0.01; Figures 1D and 1E). Furthermore, out of eight mice per group, six WT mice but only two $PHD2^{+/-}$ mice displayed gallbladder enlargement and jaundice (Figures 1D and 1E). Moreover, lymphatic metastasis was reduced by 60% in $PHD2^{+/-}$ mice (Figures 1K–1M). For subsequent studies, we used the Panc02 model, as this tumor grows and metastasizes aggressively.

$PHD2$ Haplodeficiency Impedes Intravasation of Tumor Cells

To characterize the role of PHD2 in metastasis, we analyzed tumor intravasation. Staining for the EC marker CD105 and the epithelial marker pancytokeratin revealed that tumor cell intravasation was reduced by 50% in $PHD2^{+/-}$ mice (percent of vessels with intravasated tumor cells: 48% ± 5.0% in WT versus 24% ± 0.8% in $PHD2^{+/-}$; n = 6; p < 0.001; Figures 2A and 2B). Implantation of Panc02 cells, transduced with a GFP-expressing lentiviral vector, confirmed these findings (data not shown). $PHD2$ haplodeficiency also reduced the number of circulating GFP⁺ tumor cells by 79% (Figure 2C). Instead, intravenous injection of GFP⁺ B16 tumor cells did not impair hepatic or pulmonary colonization in $PHD2^{+/-}$ mice, indicating that tumor cell lodging and extravasation in distant organs were normal (data not shown).

In addition, gene profiling revealed that tumors in $PHD2^{+/-}$ mice expressed reduced levels of prometastatic genes that promote survival, epithelial-mesenchymal transition, or motility of tumor cells, stimulate extracellular matrix degradation, or reduce cohesion between tumor-tumor or tumor-stromal cells (COX2, EGFR, HGFR, CXCR4, MMP2, MMP9, uPA, IGF1R, LOX, and N-cadherin), while expression of E-cadherin, which promotes tumor-tumor cell adhesion (Sullivan and Graham, 2007), was increased (Sullivan and Graham, 2007) (Figure 2D and Figure S5F). Notably, expression of these genes is regulated by hypoxia through HIFs (Semenza, 2003).
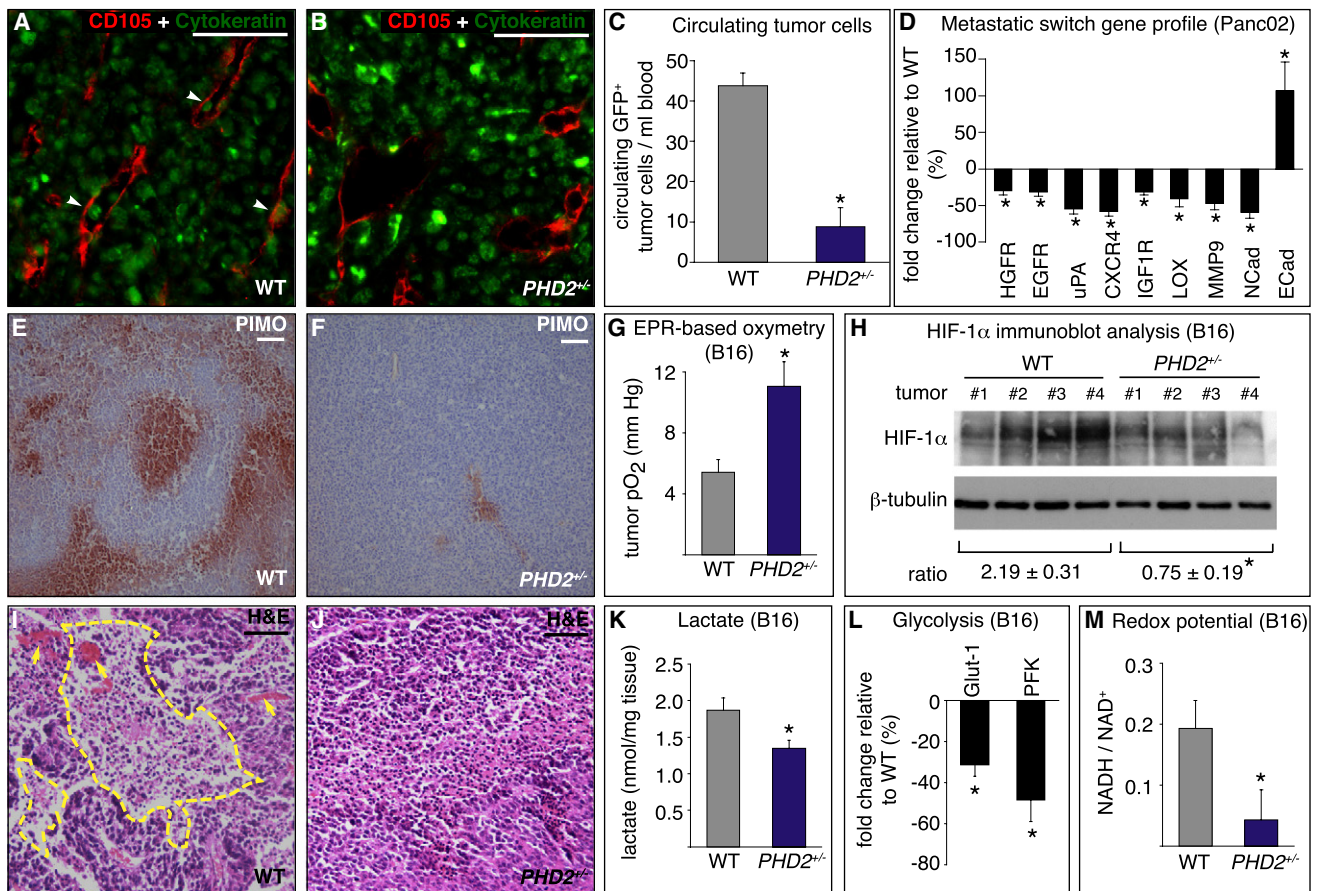
Improved Tumor Oxygenation in $PHD2^{+/-}$ Mice

Since hypoxia promotes tumor cell invasion and metastasis, we analyzed tumor oxygenation. Staining for the hypoxia-marker pimonidazole revealed a reduced hypoxic tumor area in $PHD2^{+/-}$ mice (21% ± 7% in WT versus 7% ± 3% in $PHD2^{+/-}$ for B16 tumors; n = 6; p = 0.01; Figures 2E and 2F). Electron paramagnetic resonance (EPR) oxymetry indicated that the oxygen pressure in B16 tumors was 2-fold higher in $PHD2^{+/-}$ mice (Figure 2G). In tumors in $PHD2^{+/-}$ mice, protein levels of HIF-1α were 3-fold lower (Figure 2H); levels of the HIF-target vascular endothelial growth factor (VEGF) were also reduced (μg per 10 mg tumor tissue: 4 ± 0.5 in WT versus 2.7 ± 0.2 in $PHD2^{+/-}$; n = 6; p < 0.05). Also, the necrotic tumor area was decreased in $PHD2^{+/-}$ mice (35% ± 9% in WT versus 16% ± 4% in $PHD2^{+/-}$ for B16 tumors; n = 6, p = 0.006; Figures 2I and 2J). Consistent with its hypoxia inducibility (Epstein et al., 2001; Marxsen et al., 2004), PHD3 mRNA levels in $PHD2^{+/-}$ mice were downregulated in tumors and tumor ECs freshly isolated from tumors and directly used for analysis (Figures S3I and S3J). PHD2 transcripts were also reduced in tumors in $PHD2^{+/-}$ mice, in part because of the $PHD2$ haplodeficiency of stromal cells, but likely also because of oxygen-dependent downregulation of PHD2 in tumor cells (Figure S3I). Similar results were obtained with the Panc02 tumor model (data not shown). Overall, tumors are better oxygenated in $PHD2^{+/-}$ mice.

Tumors in $PHD2^{+/-}$ Mice Show Reduced Glycolysis

Tumor cells generate ATP largely via glycolysis (Warburg effect), allowing rapid growth. The acidic microenvironment, resulting from the formation of lactate, promotes tumor invasion and malignancy. Since glycolysis is enhanced in hypoxic conditions, lactate levels are a measure of tumor metabolism and indirectly of its oxygenation. B16 tumors in $PHD2^{+/-}$ mice had lower lactate contents (Figure 2K) and expressed lower levels of the HIF-1α targets Glut-1 and PFK, key regulators of glycolytic flux (Figure 2L). Thus, tumors in $PHD2^{+/-}$ mice were less glycolytic because of improved oxygenation. Similar results were obtained for Panc02 tumors (data not shown).

Consistent with a reduced Warburg effect, tumors in $PHD2^{+/-}$ mice expressed lower levels of PDK4, which restricts entry of glycolytic intermediates into the Krebs cycle (mRNA copies per 10^3 mRNA copies β-actin: 1.60 ± 0.43 in WT versus

Figure 2. Tumor Intravasation and Oxygenation in *PHD2*$^{+/-}$ Mice

(A and B) Panc02 tumor sections stained for endothelial CD105 (red) and epithelial cytokeratin (green) revealing more intravasated tumor cells (arrowheads) in a WT (A) than *PHD2*$^{+/-}$ mice (B).

(C) Reduced circulating GFP$^+$ tumor cells in *PHD2*$^{+/-}$ mice (n = 5; p = 0.0005).

(D) RT-PCR revealing downregulation of prometastatic genes and upregulation of the anti-metastatic E-cadherin in Panc02 tumors in *PHD2*$^{+/-}$ mice (percent of WT levels; n = 5–12; p < 0.05).

(E and F) Decreased staining for pimonidazole (red) in tumors in *PHD2*$^{+/-}$ mice.

(G) EPR oxymetry revealing increased tumor oxygenation in *PHD2*$^{+/-}$ mice (n = 10; p = 0.003).

(H) Immunoblot for HIF-1α and β-tubulin revealing reduced [HIF-1α/β-tubulin] ratio in tumors in *PHD2*$^{+/-}$ mice (n = 4; p = 0.007).

(I and J) H&E staining showing necrotic area (yellow line) in a tumor of a WT (I) but not *PHD2*$^{+/-}$ mouse (J). Arrows, blood lakes.

(K–M) Reduced Warburg effect in B16 tumors in *PHD2*$^{+/-}$ mice, shown by reduced lactate content (n = 6; p = 0.04) (K), transcripts of Glut-1 and PFK (percent of WT levels; n = 5; p < 0.05) (L), and [NADH/NAD$^+$] ratio (n = 4; p < 0.05) (M).

Scale bars represent 50 μm in (A), (B), (E), (F), (I), and (J). Asterisks in (C), (D), (G), (H), and (K)–(M) denote statistical significance.

0.45 ± 0.14 in *PHD2*$^{+/-}$; n = 6-10; p = 0.03); similar findings were obtained for PDK1 (data not shown). Moreover, analysis of NAD$^+$ levels, a measure of the redox status, revealed that tumors in *PHD2*$^{+/-}$ mice shifted from glycolytic to more oxidative metabolism (μg NAD$^+$ per g tumor: 5 ± 2 in WT versus 14 ± 2 in *PHD2*$^{+/-}$; n = 4; p < 0.05); similar results were obtained when the [NADH/NAD$^+$] ratio was analyzed (Figure 2M). Overall, tumors in *PHD2*$^{+/-}$ mice were better oxygenated and adapted to more aerobic metabolism, as occurs in more benign tumors.

PHD2 Haplodeficiency Improves Vessel Function and Maturation

We then investigated how haplodeficiency of *PHD2* improved tumor oxygenation. Hypoxia in tumors may result from an insuf-ficient number of patent vessels or from supernumerary nonper-fused vessels (Thurston et al., 2007). We had expected that reduced PHD2 levels, via upregulation of HIFs, would stimulate vessel branching. However, CD31 staining revealed that tumor vessel density and vessel area were comparable in both geno-types, in all tumor models tested (Figures 3A and 3B and Figures S6A–S6D). Similar results were obtained when analyzing tumor lymphatics (Figures S6E–S6H). Also, there was no shift in tumor vessel size (Figures S6I and S6J). However, tumor vessels ap-peared more fragile in WT mice, as blood extravasated in tumors in WT but not in *PHD2*$^{+/-}$ mice (Figures 2I and 2J), explaining why tumors in WT mice appeared more reddish (Figures 1D and 1E).

We therefore analyzed whether an improvement in vessel function might explain the increased tumor oxygenation in
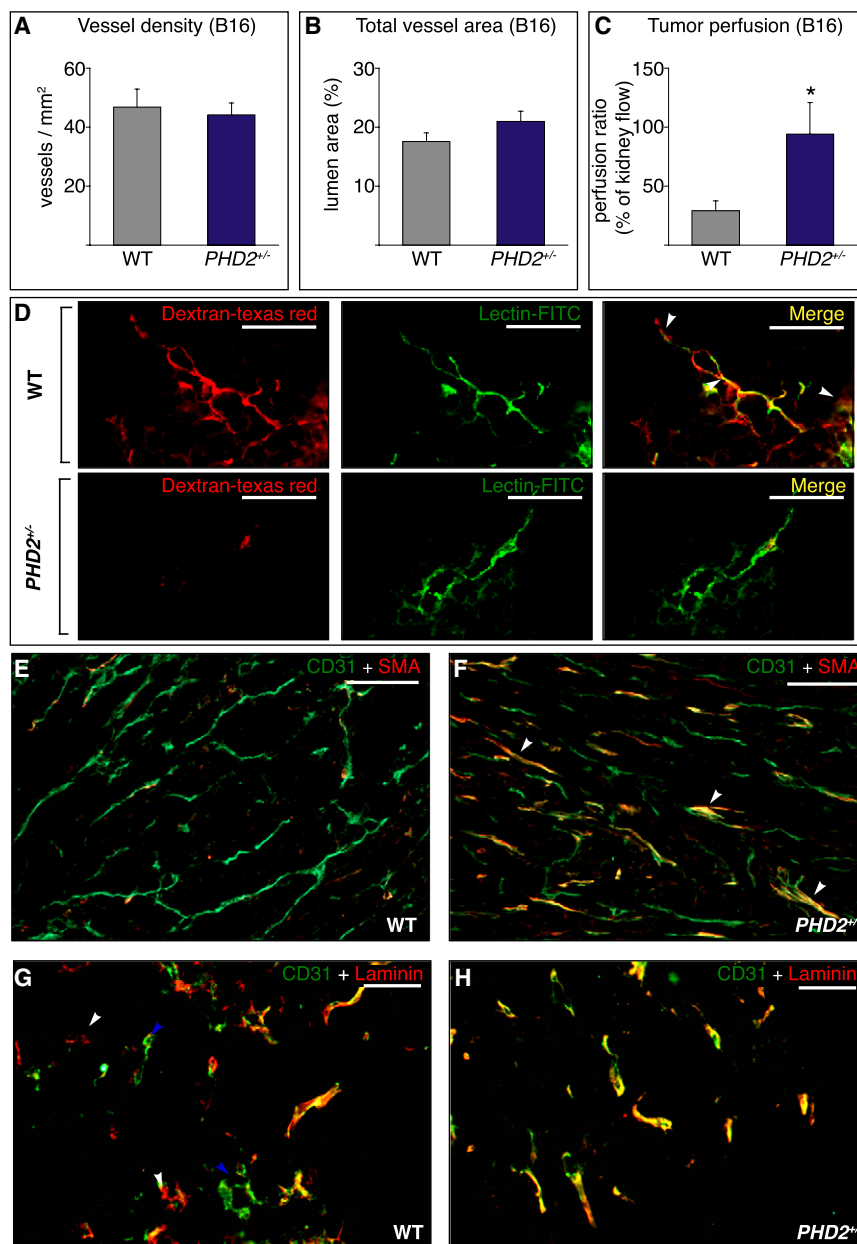
Figure 3. Improved Vessel Function and Maturation in $PHD2^{+/-}$ Mice

(A and B) Tumor vessel density (A) and vessel area (B) (n = 6; p = not significant).

(C) Improved tumor perfusion in $PHD2^{+/-}$ mice (percent of renal perfusion; n = 10; p = 0.02).

(D) Reduced tumor vessel leakiness in $PHD2^{+/-}$ mice upon injection with Texas Red-conjugated dextran (red) and FITC-conjugated lectin (green). White arrowheads on merged images indicate sites of leakage.

(E and F) Staining for CD31 (green) and αSMA (red) revealing more pericyte-covered tumor vessels (arrowheads) in $PHD2^{+/-}$ (F) than WT (E) mice.

(G and H) Staining for CD31 (green) and laminin (LAM) (red) revealing yellow "mature CD31$^+$ LAM$^+$ vessels," red "empty CD31$^-$ LAM$^+$ sleeves" (white arrowheads), and green "naked CD31$^+$ LAM$^-$ vessels" (blue arrowheads) in tumors in WT mice (G); tumors in $PHD2^{+/-}$ mice contain primarily yellow "mature CD31$^+$ LAM$^+$ vessels" (H).

Scale bars represent 50 μm in (D), (G), and (H) and 100 μm in (E) and (F). The asterisk in (C) denotes statistical significance.

11% in WT versus 23% ± 9% in $PHD2^{+/-}$; n = 4; p = 0.02; Figure 3D). Similar findings were obtained when Evans Blue was injected (Figure S8A) or transendothelial electrical resistance was measured in vitro (data not shown). Leakage of fluorescent dextran or Evans Blue in healthy vessels was normal in $PHD2^{+/-}$ mice (Figure S8). A tighter EC barrier may contribute to the reduced tumor intravasation and intratumoral bleeding in $PHD2^{+/-}$ mice.

Coverage of ECs by mural cells renders vessels more mature, tight, and stable and reduces tumor cell intravasation (Gerhardt and Semb, 2008). Double staining for CD31 and the mural marker α-smooth muscle actin (SMA) revealed that more SMA$^+$ cells covered tumor vessels in $PHD2^{+/-}$ mice (pericytes per optical field: 21.1 ± 2.0 in WT versus 31.5 ± 2.8 in $PHD2^{+/-}$; n = 5; p = 0.016; Figures 3E and 3F). ECs in stable vessels are quiescent and surrounded by a laminin (LAM)-positive basement membrane. In contrast, tumor vessels are unstable and remodel continuously; because of the hypermotility of tumor ECs, new naked vessels without basement membrane are formed, while existing vessels become denuded and regress. Hence, a fraction of tumor vessels consists of ECs surrounded by a LAM$^+$ basement membrane (referred to as "LAM$^+$ vessels"), while another fraction consists of naked ECs without LAM$^+$ basement membrane ("naked LAM$^-$ vessels"). Yet other tumor vessels persist as "empty LAM$^+$ sleeves," i.e., LAM$^+$ basement membrane channels from which ECs egressed. Hence, staining for CD31 and laminin revealed that, of all tumor vessels analyzed

$PHD2^{+/-}$ mice. Use of fluorescent microspheres revealed that perfusion of melanomas was 3-fold higher in $PHD2^{+/-}$ mice (Figure 3C). Microscopic analysis confirmed that perfusion was increased in $PHD2^{+/-}$ mice (lectin$^+$ vessels per optical field: 5.2 ± 0.5 in WT versus 7.9 ± 0.1 in $PHD2^{+/-}$; n = 4; p = 0.003). This genotypic difference was specific for tumor vessels, as healthy tissues displayed comparable vessel area, density, and perfusion in both genotypes (Figure S7).

When tumor vessels are leaky, extravasation of plasma increases the interstitial pressure, inducing vessel collapse and impeding perfusion (Jain, 2005). Upon injection of Texas Red-conjugated dextran and fluorescein isothiocyanate (FITC)-conjugated lectin, extravasation of dextran was reduced in B16 tumors in $PHD2^{+/-}$ mice (leaky vessels, percent of total: 70% ±
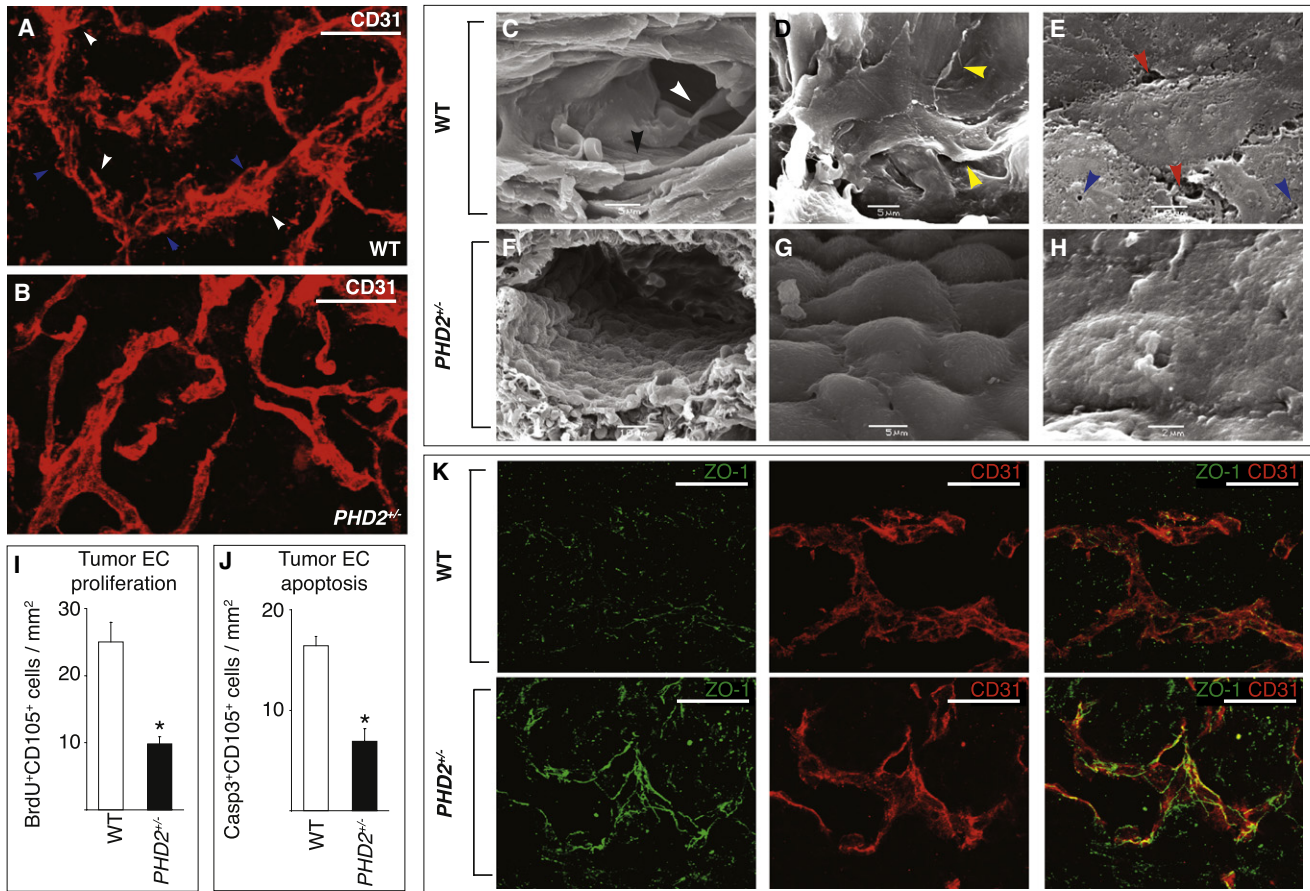
Figure 4. Endothelial Cell Normalization in *PHD2*$^{+/-}$ Mice

(A and B) Whole-mount staining of thick tumor sections for CD31 (red) revealing similar three-dimensional architecture of tumor vasculature in WT (A) and *PHD2*$^{+/-}$ (B) mice. The EC lining is discontinuous (blue arrowheads) with ECs protruding in the lumen and perivascular tumor area (white arrowheads), resulting in a hazy, thick appearance of the vessel wall in WT mice (A) but a smooth, continuous, sharply demarcated endothelial lining in *PHD2*$^{+/-}$ mice (B).

(C–H) Scanning electron microscopy of tumor vessels: in WT mice (C–E), vessels are lined by a disorganized, discontinuous, pseudostratified EC layer (black arrowhead in [C]) with ECs crawling over each other (yellow arrowheads in [D]) while forming gaps or being absent in other denuded areas (data not shown); ECs protrude filopodia-like extensions in the lumen (white arrowhead in [C]), possess numerous fenestrations (blue arrowheads in [E]), and fail to form tight cellular junctions but are separated by intercellular gaps (red arrowheads in [E]). By contrast, tumor vessels in *PHD2*$^{+/-}$ mice (F–H) are lined by a regular, orderly formed, smoothly aligned, tightly apposed, single cobblestone monolayer of "phalanx" ECs (F and G), with few fenestrations and tight intercellular junctions (H).

(I) Reduced tumor EC proliferation in *PHD2*$^{+/-}$ mice (staining for BrdU and CD105; n = 5, p < 0.001).

(J) Reduced tumor EC apoptosis in *PHD2*$^{+/-}$ mice (staining for cleaved caspase-3 and CD105; n = 5, p < 0.001).

(K) Confocal microscopy of tumor vessels in whole-mount sections, stained for ZO-1 (green) and CD31 (red), showing long ZO-1$^+$ tight junctions in *PHD2*$^{+/-}$ ECs but a scattered, discontinuous pattern of short ZO-1$^+$ tight junctions in WT cells.

Scale bars represent 25 μm in (A), (B), and (K). Asterisks in (I) and (J) denote statistical significance.

in WT mice, 68% ± 4% were LAM$^+$, 12% ± 2% were naked LAM$^-$, and the remaining 20% ± 3% were empty LAM$^+$ sleeves (n = 4; Figure 3G). By contrast, in *PHD2*$^{+/-}$ mice, up to 89% ± 2% of the vessels were LAM$^+$, while only 4% ± 2% were naked LAM$^-$ vessels, and 7% ± 1% were empty LAM$^+$ sleeves (n = 4; p < 0.0001; Figure 3H). Thus, even though tumors in *PHD2*$^{+/-}$ mice contained a similar number of vessels, vessels were more mature and stable, which could explain improved perfusion.

PHD2 Haplodeficiency Induces "Endothelial Normalization"

Whole-mount staining of thick tumor sections for CD31 revealed that the three-dimensional architecture of the tumor microvascu-

lature was comparably complex in WT and *PHD2*$^{+/-}$ mice (Figures 4A and 4B). However, in WT mice, the EC wall of tumor vessels was thick, disorganized, irregular, and often discontinuous, with holes ("honeycomb" appearance), and had ECs protruding in the lumen and perivascular stroma. In contrast, in *PHD2*$^{+/-}$ mice, the wall of tumor vessels was sharply demarcated with clearly defined boundaries and branching points and ECs forming a continuous smooth lining without protrusions, resulting in a more regular external vessel shape (Figures 4A and 4B). Thus, *PHD2* haplodeficiency did not substantially change the overall architecture of the vascular network but altered the EC lining.

Scanning electron microscopy revealed that tumor ECs in WT mice exhibited signs of a hyperactive, nonquiescent
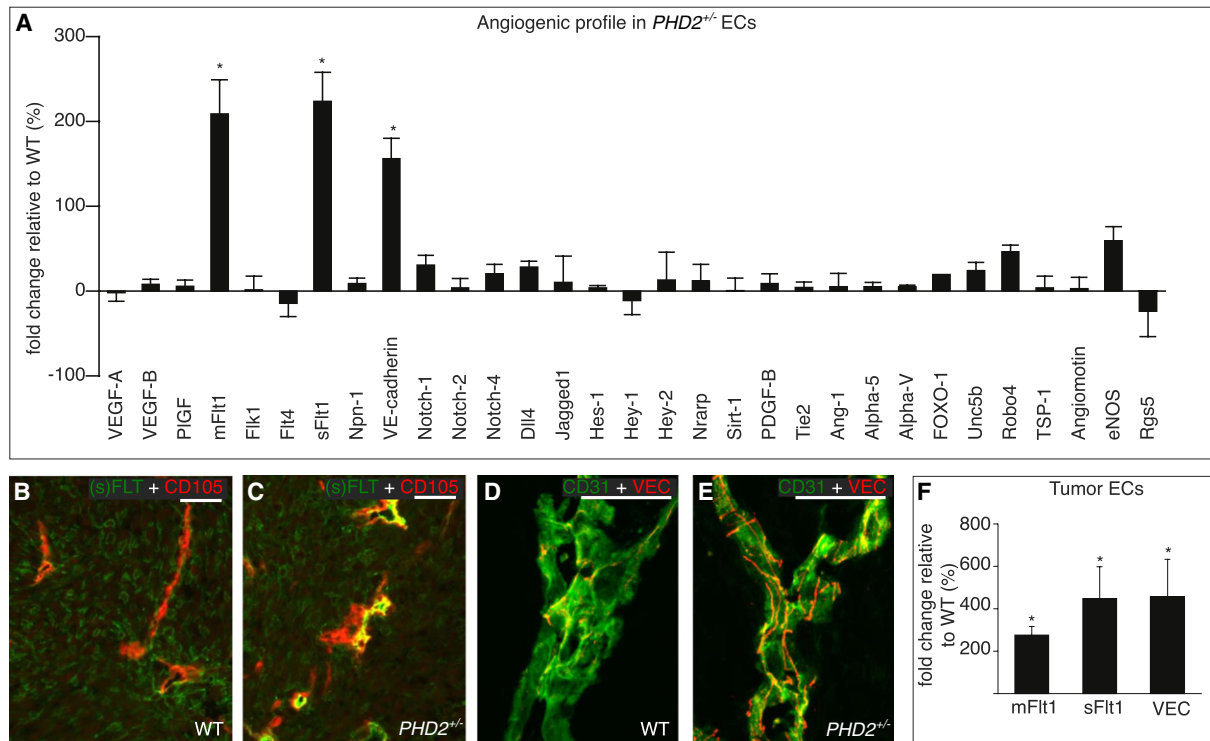
Figure 5. Enhanced (s)Flt1 and VE-Cadherin levels in *PHD2*^{+/−} Endothelial Cells

(A) RT-PCR analysis of angiogenic genes; bars represent the change in gene expression in *PHD2*^{+/−} ECs (percent of WT levels; $p < 0.01$).

(B and C) Double staining for CD105 (red) and (s)Flt1 (green) revealing stronger Flt1 signal in tumor vessels in *PHD2*^{+/−} (C) than WT (B) mice.

(D and E) Whole-mount staining for VE-cadherin (red) and CD31 (green) showing more and longer VE-cadherin[+] EC junctions in tumor vessels in *PHD2*^{+/−} (E) than WT (D) mice.

(F) RT-PCR analysis revealing elevated levels of mFlt1, sFlt1, and VE-cadherin (VEC) in tumor ECs of *PHD2*^{+/−} mice (n = 4, $p < 0.05$).

Scale bars represent 50 μm in (B) and (C) and 25 μm in (D) and (E). Asterisks in (A) and (F) denote statistical significance.
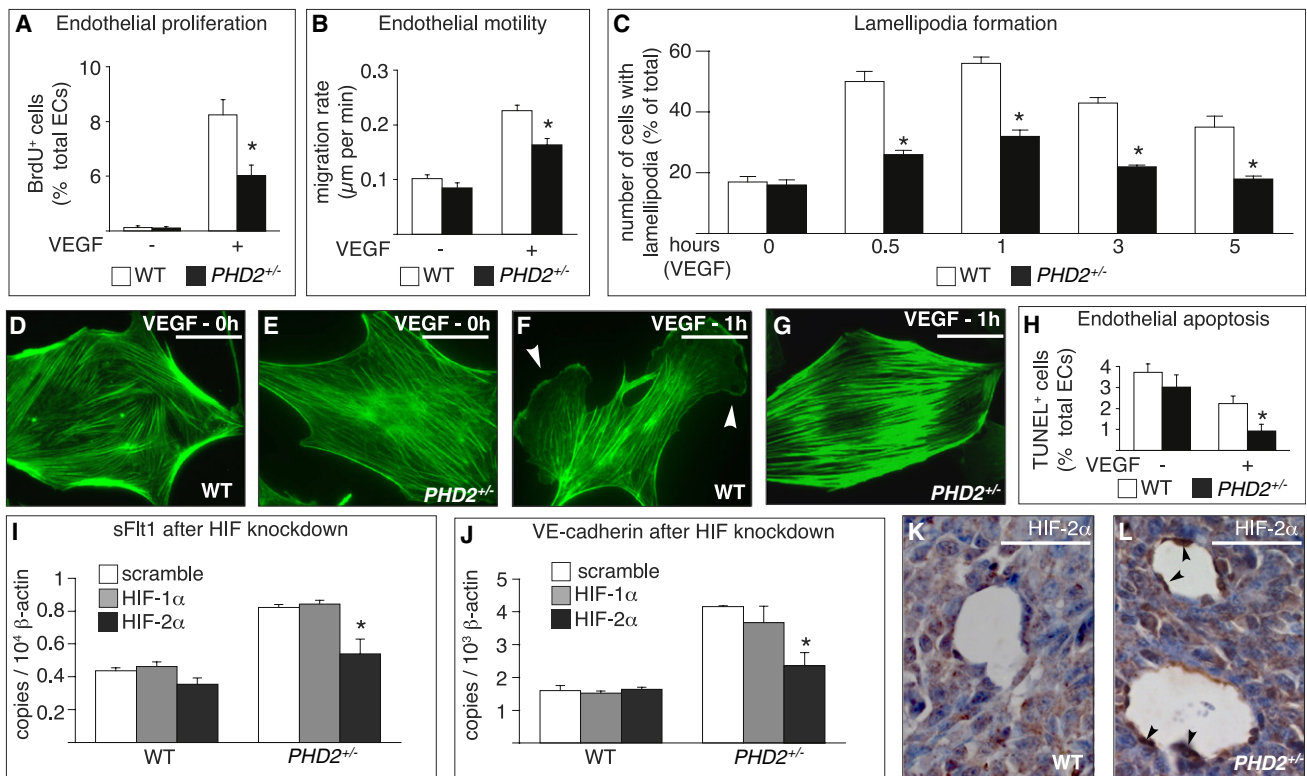
endothelium, with few signs of contact inhibition. ECs were loosely connected and detached from each other, had intercellular gaps, protruding filopodia-like extensions in the lumen, and highly fenestrated and exposed irregular cell borders, and were arranged as a pseudostratified multiple cell layer, thereby partially obstructing the lumen (Figures 4C–4E). In contrast, tumor vessels in *PHD2*^{+/−} mice were lined by a regular, orderly formed, single EC monolayer with cobblestone appearance (resembling a "phalanx" of the Greek military formation), which was continuous and tightly packed, with a normal polarity and few fenestrations (Figures 4F–4H), as a quiescent endothelium (Baluk et al., 2005; Jain, 2005). Tumor EC proliferation and apoptosis were also reduced in *PHD2*^{+/−} mice (Figures 4I and 4J). The genotypic differences in EC morphogenesis were not detected in renal and hepatic endothelium (data not shown).

Molecular analysis revealed that the EC barrier was tighter. Immunostaining for the tight junction marker ZO-1 (zona occludens) revealed that ZO-1^{+} tight junctions in tumor vessels extended over longer distances in *PHD2*^{+/−} ECs in situ (3.98 ± 0.90 μm in WT versus 4.98 ± 0.91 μm in *PHD2*^{+/−}; n = 8; $p < 0.0001$; Figure 4K). Similar findings were obtained for claudin-5 (4.7 ± 0.2 μm in WT versus 5.5 ± 0.2 μm in *PHD2*^{+/−}; n = 6; $p = 0.003$). By scanning electron microscopy, tumor vessels in

WT mice had intravascular fibrin threads and clots, which can impair perfusion. These features of increased coagulation, which can impair perfusion, were much less prevalent in *PHD2*^{+/−} mice (Figures S9A and S9B). Tumor vessels contained fewer fibrin (ogen)-immunoreactive deposits in *PHD2*^{+/−} mice (fibrin[+] area, percent of tumor area: 2.8% ± 0.4% in WT versus 1.1% ± 0.4% in *PHD2*^{+/−}; n = 6; $p = 0.01$; Figures S9C and S9D).

PHD2^{+/−} Endothelial Cells Have a Distinct Phenotype

To characterize how *PHD2* haplodeficiency regulates tumor EC phenotypes, we analyzed in confluent ECs the expression of a set of genes known to regulate EC morphogenesis. Of all candidates analyzed, soluble VEGFR-1 (sFlt1), membrane-anchored VEGFR-1 (mFlt1), and the junctional adherens molecule VE-cadherin were upregulated in *PHD2*^{+/−} cells (Figure 5A and Figures S10A and S10B). Their transcript levels were also higher in *PHD2*^{+/−} ECs when cultured at 1% O_2 (i.e., the oxygen tension in tumors) (Figures S10C–S10E). Immunostaining and RT-PCR of freshly isolated tumor ECs confirmed that (s)Flt1 and VE-cadherin were upregulated in tumor ECs in *PHD2*^{+/−} mice (Figures 5B–4F and Figures S10F–S10H). VE-cadherin was also more abundant in tumors in *PHD2*^{+/−} mice (Figure S10I). Expression for other genes involved in the specification of

A Endothelial proliferation

BrdU$^+$ cells (% total ECs)

10
8
6

VEGF   -   +
□ WT   ■ PHD2$^{+/-}$

B Endothelial motility

migration rate (μm per min)

0.3
0.2
0.1

VEGF   -   +
□ WT   ■ PHD2$^{+/-}$

C Lamellipodia formation

number of cells with lamellipodia (% of total)

60
40
20

hours (VEGF)   0   0.5   1   3   5
□ WT   ■ PHD2$^{+/-}$

D VEGF - 0h   WT

E VEGF - 0h   PHD2$^{+/-}$

F VEGF - 1h   WT

G VEGF - 1h   PHD2$^{+/-}$

H Endothelial apoptosis

TUNEL$^+$ cells (% total ECs)

4
3
2
1

VEGF   -   +
□ WT   ■ PHD2$^{+/-}$

I sFlt1 after HIF knockdown

copies / 10^4 β-actin

1
0.8
0.6
0.4
0.2

□ scramble
▨ HIF-1α
■ HIF-2α

WT   PHD2$^{+/-}$

J VE-cadherin after HIF knockdown

copies / 10^3 β-actin

5
4
3
2
1

□ scramble
▨ HIF-1α
■ HIF-2α

WT   PHD2$^{+/-}$

K HIF-2α WT

L HIF-2α PHD2$^{+/-}$

Figure 6. In Vitro Characterization of PHD2$^{+/-}$ Endothelial Cells
(A and B) Reduced proliferation (A) and motility (B) of PHD2$^{+/-}$ ECs in response to VEGF (n = 6, p < 0.05).
(C) Lamellipodia formation in response to VEGF is impaired in PHD2$^{+/-}$ ECs (n = 100 cells, p < 0.05).
(D–G) Phalloidin staining revealing comparable actin cytoskeleton in WT (D) and PHD2$^{+/-}$ (E) ECs in baseline conditions and the formation of lamellipodia (arrowheads) in a WT (F) but not in a PHD2$^{+/-}$ (G) EC upon VEGF stimulation.
(H) TUNEL staining revealing reduced apoptosis of starved PHD2$^{+/-}$ ECs in response to VEGF (n = 6; p < 0.02).
(I and J) Silencing of HIF-2α inhibits the upregulation of sFlt1 (I) and VE-cadherin (J) expression in normoxic PHD2$^{+/-}$ ECs (n = 3; p < 0.05).
(K and L) Staining of HIF-2α revealing stronger immunoreactive signal (arrowheads) in tumor ECs in PHD2$^{+/-}$ (L) than WT (K) mice.
Scale bars represent 50 μm in (D) – (G) and 25 μm in (K) and (L). Asterisks in (A)–(C) and (H) denote significance relative to WT; asterisks in (I) and (J) denote significance relative to scramble RNAi.

endothelial tip or stalk cells or angiogenesis was comparable (Figure 5A). Interestingly, levels of RGS5, a gene counteracting tumor vessel normalization (Hamzah et al., 2008), tended to be reduced, while levels of eNOS and Robo4, which promote vessel normalization (Jones et al., 2008; Kashiwagi et al., 2008), were slightly higher in PHD2$^{+/-}$ ECs (Figure 5A). PHD2 haplodeficiency did not upregulate sFlt1 in cancer-associated fibroblasts (Figures S10J and S10K).

HIF-Driven Responses of PHD2$^{+/-}$ Endothelial Cells
We then studied the response to VEGF, since elevated levels of VE-cadherin and (s)Flt1 are known to modulate this response (Carmeliet et al., 1999; Grazia Lampugnani et al., 2003; Kappas et al., 2008; Kearney et al., 2004) and VEGF inhibits vessel maturation (Greenberg et al., 2008). Proliferation and motility of PHD2$^{+/-}$ ECs were reduced upon VEGF stimulation (Figures 6A and 6B). Also, WT cells formed extensive lamellipodia and filopodia, with polarized reorganization of the actin cytoskeleton (Figures 6C and 6F and Figures S11A, S11G, and S11H; Movie S1), while PHD2$^{+/-}$ cells failed to do so (Figures 6C and 6G and

Figures S11A, S11G, and S11I; Movie S2). This defect was specific for VEGF, as the response to FGF-2 was normal in PHD2$^{+/-}$ cells (Figures S11B–S11G). The corneal neovascularization response to FGF-2 was also preserved in PHD2$^{+/-}$ mice (data not shown). Apoptosis, induced by serum deprivation, was reduced in PHD2$^{+/-}$ ECs, slightly in baseline conditions, and, more significantly, upon stimulation with VEGF (Figure 6H). Overall, PHD2$^{+/-}$ ECs were less responsive to the mitogenic and migratory activity of VEGF while being more sensitive to its survival activity.

Furthermore, silencing in vitro the expression of HIF-1α or HIF-2α by more than 80% (data not shown) showed that the upregulation of sFlt1 and VE-cadherin in PHD2$^{+/-}$ ECs was inhibited primarily by silencing HIF-2α in normoxic conditions (Figures 6I and 6J), while silencing of HIF-1α also contributed in hypoxic conditions, albeit at a lower level (data not shown). Immunostaining revealed a stronger signal for HIF-2α in tumor vessels in PHD2$^{+/-}$ mice (HIF-2α^+ tumor vessels, percent of vessels with lumen: 30% ± 6% in WT versus 49% ± 4% in PHD2$^{+/-}$; n = 4; p = 0.04; Figures 6K and 6L).
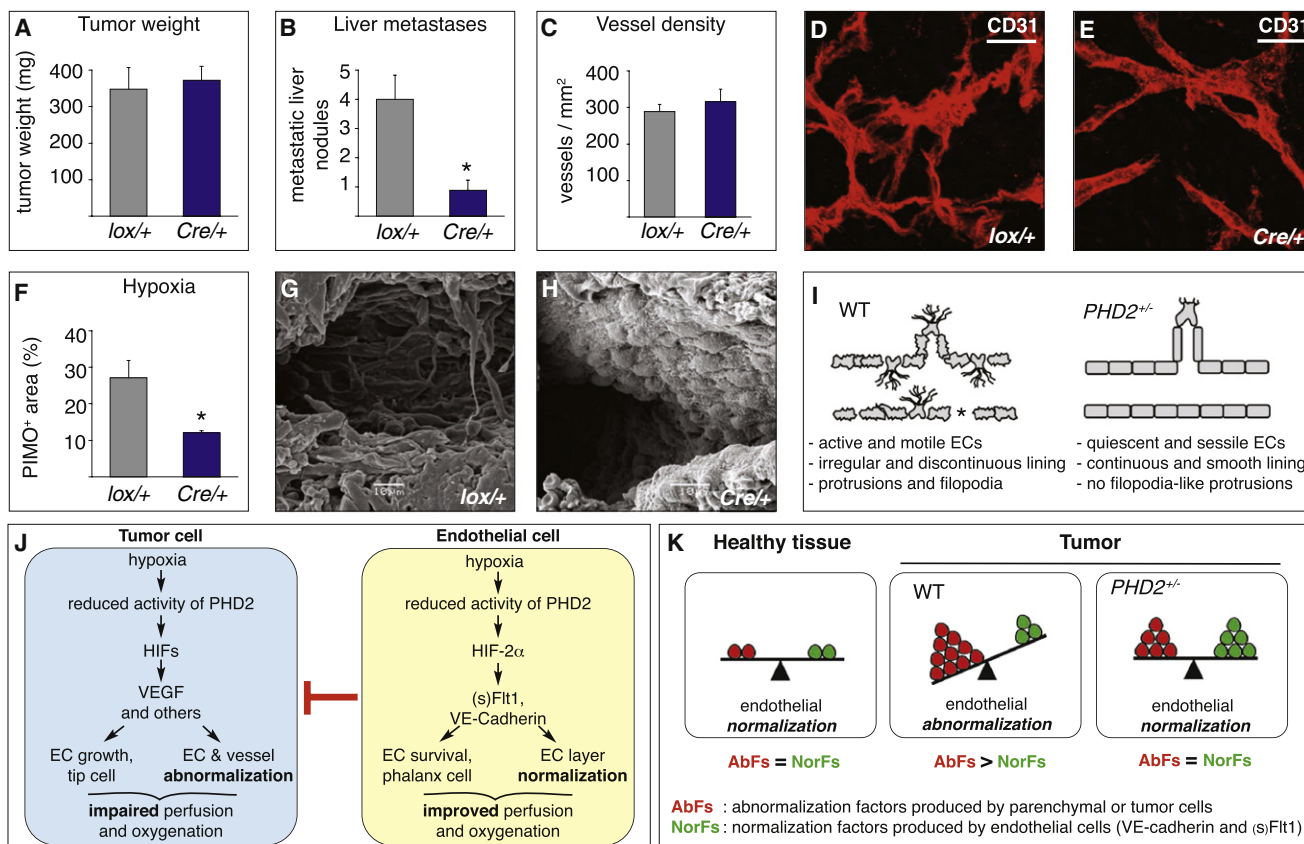
Figure 7. Phenotypic Characterization of *PHD2^Cre/+* Mice

(A–H) Phenotype of *PHD2^Cre/+* mice with endothelial *PHD2* haplodeficiency (*Cre*/+) and *PHD2^lox/+* (*lox*/+) control littermates. Panc02 tumor weight (A), vessel density (C), and microvascular architecture (D and E) are comparable, but metastasis (B) and hypoxia (F) are reduced in *PHD2^Cre/+* mice (n = 10; p < 0.05). Whole-mount CD31 staining and scanning electron microscopy reveal that, in contrast to *PHD2^lox/+* mice (D and G), the tumor endothelial layer is normalized in *PHD2^Cre/+* mice (E and H) (see Figures 4F–4H for comparison).

(I) Scheme of key EC phenotypes. In abnormalized tumor vessels in WT mice, hypermotile endothelial tip-like cells protrude filopodia in the lumen and perivascular stroma, and abnormally shaped ECs (irregular cell border) form a pseudostratified, loosely attached layer, while other vessel areas become denuded (asterisk). In more normalized tumor vessels in *PHD2^+/−* mice, ECs shift to a phalanx-like phenotype (smooth, regular cell border) characterized by EC survival, tightness, and quiescence, which improves tissue perfusion and oxygen delivery. For reasons of clarity and simplicity, not all phenotypic features (such as for instance, coverage by mural cells) are depicted.

(J) PHD2 model. Left: hypoxic tumor cells induce endothelial abnormalization by release of VEGF and other abnormalization factors, which impairs perfusion and causes hypoxia. Right: ECs counteract this abnormalization switch, in part through upregulation of (s)Flt1 and VE-Cadherin, thereby improving vessel perfusion and oxygenation. This pathway is more effective in *PHD2^+/−* mice because endothelial *PHD2* haplodeficiency resets oxygen sensing and makes them better (pre)-adapted to hypoxia.

(K) Scheme of the *endothelial abnormalization switch*. Left: In healthy tissues, the production of abnormalization factors (AbFs) by (nonendothelial) parenchymal cells is in balance with the production of normalization factors (NorFs) by ECs, resulting in EC normalization. Middle: In tumors in WT mice, excess production of tumor cell-derived AbFs over EC-derived NorFs tilts the balance in favor of EC abnormalization. Right: In tumors in *PHD2^+/−* mice, haplodeficiency of *PHD2* upregulates the production of NorFs by ECs, thereby counteracting EC abnormalization; the resultant improved oxygenation lowers the production of AbFs by tumor cells, overall re-equilibrating the balance in favor of EC normalization.

Scale bars represent 50 μm in (F) and (G). Asterisks in (B) and (F) denote statistical significance.

Endothelial Haplodeficiency of *PHD2* Induces Endothelial Normalization

To confirm the role of PHD2 in ECs in vivo, we generated conditional *PHD2* haplodeficient mice (*PHD2^Cre/+*) lacking a single PHD2 allele in ECs by intercrossing *PHD2^lox/+* mice with *Tie2:Cre* mice. Analysis of *PHD2^Cre/+* mice revealed that EC haplodeficiency of *PHD2* sufficed to phenocopy the key findings in *PHD2^+/−* mice. Indeed, primary tumor growth was comparable, but metastasis was reduced (Figures 7A and 7B), while tumor vessel density (Figure 7C), area (data not shown), and architecture (Figures 7D and 7E) were comparable. However, tumors were better oxygenated (Figure 7F), and tumor vessels showed the cardinal morphological signs of EC normalization (Figures 7D, 7E, 7G, and 7H). Further, general *PHD2* haplodeficiency did not alter the accumulation of inflammatory cells and cancer-associated fibroblasts (data not shown). These conditional knockout studies do not rule out a possible role for leukocyte or fibroblast PHD2 in tumor biology.

DISCUSSION

This study identifies a basic biological role for endothelial PHD2 in oxygen delivery by regulating vessel morphogenesis. Our data suggest a model whereby a decrease in the activity of PHD2 in ECs in hypoxia counteracts abnormalization of the EC layer. This involves a shift from an endothelial tip to a distinct phenotype, referred to here as the "phalanx phenotype," and relies in part on HIF-mediated upregulation of (s)Flt1 and VE-cadherin. EC normalization provides a feedback mechanism for vessels to readjust their shape, not number, in order to optimize oxygen supply when the latter is insufficient.

In healthy tissues, "productive" angiogenesis generates perfused blood vessels and improves oxygenation. By contrast, tumor angiogenesis is often "nonproductive" as vessel abnormalization impairs oxygen supply (Jain, 2005). The importance of vessel normalization for tumor growth and treatment is being increasingly recognized, but its relevance for metastasis remained unknown (Hamzah et al., 2008; Kashiwagi et al., 2008; Stockmann et al., 2008; Winkler et al., 2004). *PHD2* haplodeficiency promoted endothelial rather than vessel normalization (Figure 7I). The resultant tightened endothelial barrier, improved tumor oxygenation, and downregulation of metastatic genes can explain why *PHD2* haplodeficiency suppressed tumor invasion, intravasation, and metastasis. Thus, a change in endothelial shape, even without alterations in vessel numbers, sufficed to induce a shift to reduced malignancy and metastasis.

Hypoxic cancer cells stimulate angiogenesis by upregulating factors such as VEGF (Semenza, 2003); this response is controlled by PHD2 (Lee et al., 2008). When released by tumor cells in excess, these angiogenic factors turn into EC "abnormalization factors" (AbFs), which induce nonproductive abnormalized vessels. This may initiate a vicious self-sustaining cycle in which EC abnormalization impairs tumor perfusion and aggravates hypoxia, which will then upregulate AbFs in tumor cells even more and, in turn, amplify EC abnormalization again. $PHD2^{+/-}$ ECs counteract this process by reinstalling EC normalization (or preventing its abnormalization altogether). Indeed, they upregulate EC "normalization factors" (NorFs) such as (s)Flt1 and VE-cadherin, which antagonize the activity of AbFs. EC normalization in turn will increase tumor oxygenation, and interrupt the vicious cycle of EC abnormalization, driven by hypoxic tumor cells. Together, WT tumor cells induce vessel abnormalization and impair oxygen supply, while $PHD2^{+/-}$ ECs counteract this process in a negative feedback and readjust oxygen supply by promoting endothelial normalization. A reduction of PHD2 activity by hypoxia in WT ECs will also trigger the EC normalization program, but less efficiently than haplodeficiency of *PHD2* (see below). This model is schematically illustrated in Figures 7J and 7K.

The responses of endothelial and tumor cells to hypoxia are tightly linked, since the activity of PHD2 coordinately changes in function of the oxygen tension. Thus, when oxygen levels drop (and decrease the activity of PHD2 in tumor and ECs), the *absolute* levels of AbFs and NorFs will coordinately rise. Since tumor cells produce more AbFs than ECs produce NorFs, their *relative* balance likely even tilts over to more EC abnormalization in severe hypoxic conditions. This may explain why hypoxic

suppression of PHD2 in ECs in WT mice cannot overcome the strong abnormalization response by tumor cells. By rendering ECs better preadapted to hypoxia than tumor cells, haplodeficiency of *PHD2 re-equilibrates* this balance in favor of the EC normalization response; this indirectly affects tumor cells as well, since, as a result of the improved oxygenation, tumor cells will now also produce fewer AbFs (Figure 7K). This model therefore predicts that pharmacological inhibition of PHD2 specifically in ECs may also induce vessel normalization. In physiological conditions, the *relative* balance between EC abnormalization and normalization is more in equilibrium (Figure 7K). Ongoing studies suggest that *PHD2* haplodeficiency also normalizes vessels in other pathological conditions, suggesting that it has a more general role than in cancer alone (M.M. and P.C., unpublished data).

PHD2 haplodeficiency did not affect the number of tumor vessels. This may seem paradoxical to the observation that the migratory and mitogenic responses of $PHD2^{+/-}$ ECs to VEGF are impaired. However, these impaired responses are balanced off by an increased survival response to VEGF, while their responsiveness to other molecules (such as FGF-2) is still preserved. Also, an increased EC motility may not necessarily generate more vessels. We speculate that hypermotile WT ECs "move around" and leave their resident position more often. As a result, existing vessels become denuded and regress, while new naked vessels are formed coincidently. When both processes are in balance, tumor vessel density remains unchanged. By contrast, $PHD2^{+/-}$ ECs are more sessile and, once lining a vessel, "stay put," thereby reducing nonproductive remodeling of vessel regression and sprouting. Hence, by being more "passive" and quiescent, $PHD2^{+/-}$ tumor vessels maintain their numbers.

Upregulation of VE-cadherin is a likely mechanism underlying EC normalization. Indeed, VE-cadherin inhibits EC proliferation and apoptosis and tightens the barrier (Carmeliet et al., 1999; Taddei et al., 2008). It also induces a "normalized, stabilized, quiescent" EC phenotype indirectly by inhibiting proliferation and promoting survival in response to VEGF (Carmeliet et al., 1999; Grazia Lampugnani et al., 2003). The VEGF-trap sFlt1 also participates in fine-tuning EC normalization. Interestingly, a pericellular gradient of sFlt1 improves vessel morphogenesis more than mFlt1 (Kappas et al., 2008; Kearney et al., 2004). It remains to be determined how PHD2 interacts with other "normalization" pathways, such as nitric oxide, Tie2, MMPs, myeloid-derived VEGF, Rgs5, and PDGFR-β (Greenberg et al., 2008; Hamzah et al., 2008; Kashiwagi et al., 2008; Stockmann et al., 2008; Winkler et al., 2004).

Endothelial tip and stalk cells each have their own molecular signature (Gerhardt et al., 2003; Hellstrom et al., 2007). Phalanx cells might represent another type of ECs with a distinct identity: unlike tip cells, they extend few filopodia and migrate poorly in response to VEGF, form a tight barrier and vascular lumen, and express elevated levels of (s)Flt1 and VE-cadherin. They resemble stalk cells by depositing basement membrane and establishing junctions but differ by their increased quiescence and reduced mitogenic response to VEGF. We speculate that these three EC phenotypes should not be considered as nonoverlapping identities, but, more likely, as belonging to a spectrum of

phenotypes, whereby tip and phalanx cells represent the extreme examples of either the most navigatory or the most sedentary, quiescent cell type. Possibly, even though some of the genes are expressed by each of the three cell types, different threshold levels or qualitative signaling properties may specify each cell type.

Our data suggest that HIF-2α is involved in EC normalization. Consistent herewith, reduction of HIF-2α impairs vessel morphogenesis (Peng et al., 2000) and induces aberrant vascular networks (Yamashita et al., 2008). Also, HIF-2α binds to hypoxia-responsive elements in the *VE-cadherin* and *Flt1* promoter in ECs (Dutta et al., 2008; Le Bras et al., 2007). Moreover, since HIF-2α is relatively resistant to degradation at oxygen levels that normally lead to degradation of HIF-1α (Lofstedt et al., 2007), it may be relevant in maintaining vessel normalization in better oxygenated (normalized) vessels. Nonetheless, given the dynamically changing tumor oxygen microenvironment, we cannot exclude that upregulation of HIF-1α may also contribute to vessel normalization.

Implantation of fibroblasts, in which PHD2 expression was completely silenced, stimulates angiogenesis in healthy WT mice through release of angiogenic factors (Wu et al., 2008). In another study, inducible broad-spectrum inactivation of *PHD2* after birth (*PHD2^{IND−KO}*) induced growth of supernumerary vessels in healthy organs (Takeda et al., 2008; Takeda et al., 2007). It remains unclear whether the vascular changes in *PHD2^{IND−KO}* mice are secondary to the high hematocrit levels, hyperviscosity, thrombosis, and cardiac dysfunction or to elevated circulating VEGF levels (Minamishima et al., 2008; Takeda et al., 2007). An alternative explanation may relate to the hydroxylation-independent activity of PHD2, but this effect has been only identified in immortalized ECs so far (Takeda and Fong, 2007). Since only complete *PHD2* inactivation caused *spontaneous* vessel changes, PHD2 controls vessel number versus morphogenesis in a gene dosage-dependent manner.

Finally, our findings suggest possible medical implications. By normalizing the tumor vasculature, endothelial haplodeficiency of *PHD2* may shift tumors to a less malignant, metastasizing phenotype. As oxygenation levels determine responsiveness to irradiation and chemotherapy, inhibition of PHD2 might improve anticancer therapy (M.M. and P.C., unpublished data). PHD2 inhibitors may represent an unanticipated class of antivascular agents that, in contrast to traditional antiangiogenic therapy, regulate vessel shape but not size or number. As quiescent vessels in healthy tissues are not affected in *PHD2^{+/−}* mice, inhibition of PHD2 selectively targets tumor vessels. Obviously, before any conclusion that PHD2 inhibitors might be useful for anticancer therapy is drawn, these findings should be confirmed in spontaneous tumor models. Also, strategies to deliver such compounds selectively to ECs should be explored, and the consequences of inhibiting PHD2 in malignant cells will need to be carefully analyzed, as silencing of PHD2 may evoke both oncogenic and tumor-suppressor effects on tumor cells or upregulate vessel abnormalization factors in tumor cells (Couvelard et al., 2008; Lee et al., 2008; Wu et al., 2008). At this stage, our studies provide insight in how oxygen sensors help to shape the microvasculature for one of its most important functions, i.e., supplying oxygen to cells.

EXPERIMENTAL PROCEDURES

Syngeneic Tumor Models

Five hundred thousand B16F10.9 melanoma and 10^5 Lewis lung carcinoma cells were injected subcutaneously into the right flank or foot pad, respectively. Tumor volumes were measured every 2 days with a caliper with the formula: $V = \pi \times [d^2 \times D] / 6$, where d is the minor tumor axis and D is the major tumor axis. One million Panc02 tumor cells were injected into the head of the pancreas; tumors were weighed after 10 days. Circulating tumor cells were scored on 1 ml of peripheral blood upon red blood cell lysis.

Histology and Electron Microscopy

All methods for histology and immunostaining have been described (Fischer et al., 2007). For scanning electron microscopy analysis, mice were perfused with 2% paraformaldehyde (PFA) and 2.5% glutaraldehyde in 0.1 M Na-cacodylate buffer for 7 min. Organs were dissected, cross-sectioned, and fixed o/n in the same solution. Samples were postfixed with 2% osmiumtetroxide and dehydrated in a graded aceton series, critical-point dried (Balzers CPD 030), mounted on stubs, and coated with gold (SPI-MODULE Sputter Coater, SPI Supplies). Images were obtained with a scanning electron microscope (JEOL JSM-6360) at 15 kV.

In Vitro Biological Assays

ECs were derived from lungs as described (Kuhlencordt et al., 2004). For the proliferation and apoptosis assay, 5×10^5 ECs were seeded in gelatin-coated 24-well plate. Subconfluent cell layers were either not stimulated or were stimulated with 50 ng/ml VEGF. Proliferation was assessed upon BrdU incorporation and staining with FITC-conjugated anti-BrdU. Apoptosis was assayed by TUNEL staining. For the motility assay, confluent cell layers seeded on a fibronectin-coated 35 mm tissue culture dish were scratched in the absence or presence of VEGF or FGF-2 (50 ng/ml). Images were acquired for 6–14 hr with an image taken every 15 min. Quantification of lamellipodia and filopodia was performed as described (Kitamura et al., 2008).

Expression Analysis

The following antibodies were used: rabbit anti-PHD1 (P. Ratcliffe), rabbit anti-PHD2 (P. Maxwell; Novus), rabbit anti-PHD3 (Novus), rabbit anti-HIF-1, rabbit anti-HIF-2 (Novus), goat anti-VE-cadherin (R&D Systems), and rabbit anti-β-tubulin or anti-β-actin (Abcam). sFlt1 was measured by immunoassays (R&D Systems). Quantitative RT-PCR was performed as described (Fischer et al., 2007). For Assay ID (Applied Biosystems) and sequence of primers and probes, see Table S2.

Hypoxia Assessment and Tumor Perfusion

Tumor hypoxia and perfusion were analyzed as described (Fischer et al., 2007). Vessel leakage was analyzed after intravenous coinjection of 0.25 mg Texas Red-conjugated Dextran 70 kD (Molecular Probes) and 0.05 mg FITC-labeled lectin (*Lycopersicon esculentum*; Vector Laboratories). Ten minutes later, mice were perfused with saline and 2% PFA. Tumors were then harvested and frozen in optimum cutting temperature compound.

Oxymetry, Lactate, and Redox Potential

Tumor oxygen tension (pO$_2$) was measured through the use of charcoal powder (100 μg; CX0670-1; EM Science) as the O$_2$-sensitive probe and EPR spectrometer (Magnetech). Lactate concentration and [NADH/NAD$^+$] ratio were measured as described (Pospisilik et al., 2007).

Statistics

Data represent mean ± SEM of representative experiments unless otherwise stated. Statistical significance was calculated by t test or two-way ANOVA where indicated (Prism v4.0b), with $p < 0.05$ considered statistically significant.

SUPPLEMENTAL DATA

Supplemental Data include Supplemental Experimental Procedures, 11 figures, two tables, and two movies and can be found with this article online at http://www.cell.com/supplemental/S0092-8674(09)00068-3.

REFERENCES

Baluk, P., Hashizume, H., and McDonald, D.M. (2005). Cellular abnormalities of blood vessels as targets in cancer. Curr. Opin. Genet. Dev. *15*, 102–111.

Bergers, G., and Hanahan, D. (2008). Modes of resistance to anti-angiogenic therapy. Nat. Rev. Cancer *8*, 592–603.

Carmeliet, P., Lampugnani, M.G., Moons, L., Breviario, F., Compernolle, V., Bono, F., Balconi, G., Spagnuolo, R., Oostuyse, B., Dewerchin, M., et al. (1999). Targeted deficiency or cytosolic truncation of the VE-cadherin gene in mice impairs VEGF-mediated endothelial survival and angiogenesis. Cell *98*, 147–157.

Couvelard, A., Deschamps, L., Rebours, V., Sauvanet, A., Gatter, K., Pezzella, F., Ruszniewski, P., and Bedossa, P. (2008). Overexpression of the oxygen sensors PHD-1, PHD-2, PHD-3, and FIH Is associated with tumor aggressiveness in pancreatic endocrine tumors. Clin. Cancer Res. *14*, 6634–6639.

Dutta, D., Ray, S., Vivian, J.L., and Paul, S. (2008). Activation of the VEGFR1 chromatin domain: An angiogenic signal-ETS1/HIF-2alpha regulatory axis. J. Biol. Chem. *283*, 25404–25413.

Epstein, A.C., Gleadle, J.M., McNeill, L.A., Hewitson, K.S., O'Rourke, J., Mole, D.R., Mukherji, M., Metzen, E., Wilson, M.I., Dhanda, A., et al. (2001). C. elegans EGL-9 and mammalian homologs define a family of dioxygenases that regulate HIF by prolyl hydroxylation. Cell *107*, 43–54.

Fischer, C., Jonckx, B., Mazzone, M., Zacchigna, S., Loges, S., Pattarini, L., Chorianopoulos, E., Liesenborghs, L., Koch, M., De Mol, M., et al. (2007). Anti-PlGF inhibits growth of VEGF(R)-inhibitor-resistant tumors without affecting healthy vessels. Cell *131*, 463–475.

Gerhardt, H., and Semb, H. (2008). Pericytes: gatekeepers in tumour cell metastasis? J. Mol. Med. *86*, 135–144.

Gerhardt, H., Golding, M., Fruttiger, M., Ruhrberg, C., Lundkvist, A., Abramsson, A., Jeltsch, M., Mitchell, C., Alitalo, K., Shima, D., et al. (2003). VEGF guides angiogenic sprouting utilizing endothelial tip cell filopodia. J. Cell Biol. *161*, 1163–1177.

Grazia Lampugnani, M., Zanetti, A., Corada, M., Takahashi, T., Balconi, G., Breviario, F., Orsenigo, F., Cattelino, A., Kemler, R., Daniel, T.O., et al. (2003). Contact inhibition of VEGF-induced proliferation requires vascular endothelial cadherin, beta-catenin, and the phosphatase DEP-1/CD148. J. Cell Biol. *161*, 793–804.

Greenberg, J.I., Shields, D.J., Barillas, S.G., Acevedo, L.M., Murphy, E., Huang, J., Scheppke, L., Stockmann, C., Johnson, R.S., Angle, N., et al. (2008). A role for VEGF as a negative regulator of pericyte function and vessel maturation. Nature *456*, 809–813.

Hamzah, J., Jugold, M., Kiessling, F., Rigby, P., Manzur, M., Marti, H.H., Rabie, T., Kaden, S., Grone, H.J., Hammerling, G.J., et al. (2008). Vascular normalization in Rgs5-deficient tumours promotes immune destruction. Nature *453*, 410–414.

Hellstrom, M., Phng, L.K., Hofmann, J.J., Wallgard, E., Coultas, L., Lindblom, P., Alva, J., Nilsson, A.K., Karlsson, L., Gaiano, N., et al. (2007). Dll4 signalling through Notch1 regulates formation of tip cells during angiogenesis. Nature *445*, 776–780.

Jain, R.K. (2005). Normalization of tumor vasculature: an emerging concept in antiangiogenic therapy. Science *307*, 58–62.

Jones, C.A., London, N.R., Chen, H., Park, K.W., Sauvaget, D., Stockton, R.A., Wythe, J.D., Suh, W., Larrieu-Lahargue, F., Mukouyama, Y.S., et al. (2008). Robo4 stabilizes the vascular network by inhibiting pathologic angiogenesis and endothelial hyperpermeability. Nat. Med. *14*, 448–453.

Kaelin, W.G., Jr., and Ratcliffe, P.J. (2008). Oxygen sensing by metazoans: the central role of the HIF hydroxylase pathway. Mol. Cell *30*, 393–402.

Kappas, N.C., Zeng, G., Chappell, J.C., Kearney, J.B., Hazarika, S., Kallianos, K.G., Patterson, C., Annex, B.H., and Bautch, V.L. (2008). The VEGF receptor Flt-1 spatially modulates Flk-1 signaling and blood vessel branching. J. Cell Biol. *181*, 847–858.

Kashiwagi, S., Tsukada, K., Xu, L., Miyazaki, J., Kozin, S.V., Tyrrell, J.A., Sessa, W.C., Gerweck, L.E., Jain, R.K., and Fukumura, D. (2008). Perivascular nitric oxide gradients normalize tumor vasculature. Nat. Med. *14*, 255–257.

Kearney, J.B., Kappas, N.C., Ellerstrom, C., DiPaola, F.W., and Bautch, V.L. (2004). The VEGF receptor flt-1 (VEGFR-1) is a positive modulator of vascular sprout formation and branching morphogenesis. Blood *103*, 4527–4535.

Kitamura, T., Asai, N., Enomoto, A., Maeda, K., Kato, T., Ishida, M., Jiang, P., Watanabe, T., Usukura, J., Kondo, T., et al. (2008). Regulation of VEGF-mediated angiogenesis by the Akt/PKB substrate Girdin. Nat. Cell Biol. *10*, 329–337.

Kuhlencordt, P.J., Rosel, E., Gerszten, R.E., Morales-Ruiz, M., Dombkowski, D., Atkinson, W.J., Han, F., Preffer, F., Rosenzweig, A., Sessa, W.C., et al. (2004). Role of endothelial nitric oxide synthase in endothelial activation: insights from eNOS knockout endothelial cells. Am. J. Physiol. Cell Physiol. *286*, C1195–C1202.

Le Bras, A., Lionneton, F., Mattot, V., Lelievre, E., Caetano, B., Spruyt, N., and Soncin, F. (2007). HIF-2alpha specifically activates the VE-cadherin promoter independently of hypoxia and in synergy with Ets-1 through two essential ETS-binding sites. Oncogene *26*, 7480–7489.

Lee, K.A., Lynd, J.D., O'Reilly, S., Kiupel, M., McCormick, J.J., and LaPres, J.J. (2008). The biphasic role of the hypoxia-inducible factor prolyl-4-hydroxylase, PHD2, in modulating tumor-forming potential. Mol. Cancer Res. *6*, 829–842.

Lofstedt, T., Fredlund, E., Holmquist-Mengelbier, L., Pietras, A., Ovenberger, M., Poellinger, L., and Pahlman, S. (2007). Hypoxia inducible factor-2alpha in cancer. Cell Cycle *6*, 919–926.

Marxsen, J.H., Stengel, P., Doege, K., Heikkinen, P., Jokilehto, T., Wagner, T., Jelkmann, W., Jaakkola, P., and Metzen, E. (2004). Hypoxia-inducible factor-1 (HIF-1) promotes its degradation by induction of HIF-alpha-prolyl-4-hydroxylases. Biochem. J. *381*, 761–767.

Milkiewicz, M., Pugh, C.W., and Egginton, S. (2004). Inhibition of endogenous HIF inactivation induces angiogenesis in ischaemic skeletal muscles of mice. J. Physiol. *560*, 21–26.

Minamishima, Y.A., Moslehi, J., Bardeesy, N., Cullen, D., Bronson, R.T., and Kaelin, W.G., Jr. (2008). Somatic inactivation of the PHD2 prolyl hydroxylase causes polycythemia and congestive heart failure. Blood *111*, 3236–3244.

Nangaku, M., Izuhara, Y., Takizawa, S., Yamashita, T., Fujii-Kuriyama, Y., Ohneda, O., Yamamoto, M., van Ypersele de Strihou, C., Hirayama, N., and Miyata, T. (2007). A novel class of prolyl hydroxylase inhibitors induces angiogenesis and exerts organ protection against ischemia. Arterioscler. Thromb. Vasc. Biol. *27*, 2548–2554.

Peng, J., Zhang, L., Drysdale, L., and Fong, G.H. (2000). The transcription factor EPAS-1/hypoxia-inducible factor 2alpha plays an important role in vascular remodeling. Proc. Natl. Acad. Sci. USA *97*, 8386–8391.

Pospisilik, J.A., Knauf, C., Joza, N., Benit, P., Orthofer, M., Cani, P.D., Ebersberger, I., Nakashima, T., Sarao, R., Neely, G., et al. (2007). Targeted

deletion of AIF decreases mitochondrial oxidative phosphorylation and protects from obesity and diabetes. Cell *131*, 476–491.

Semenza, G.L. (2003). Targeting HIF-1 for cancer therapy. Nat. Rev. Cancer *3*, 721–732.

Stockmann, C., Doedens, A., Weidemann, A., Zhang, N., Takeda, N., Greenberg, J.I., Cheresh, D.A., and Johnson, R.S. (2008). Deletion of vascular endothelial growth factor in myeloid cells accelerates tumorigenesis. Nature *456*, 814–818.

Sullivan, R., and Graham, C.H. (2007). Hypoxia-driven selection of the metastatic phenotype. Cancer Metastasis Rev. *26*, 319–331.

Taddei, A., Giampietro, C., Conti, A., Orsenigo, F., Breviario, F., Pirazzoli, V., Potente, M., Daly, C., Dimmeler, S., and Dejana, E. (2008). Endothelial adherens junctions control tight junctions by VE-cadherin-mediated upregulation of claudin-5. Nat. Cell Biol. *10*, 923–934.

Takeda, K., and Fong, G.H. (2007). Prolyl hydroxylase domain 2 protein suppresses hypoxia-induced endothelial cell proliferation. Hypertension *49*, 178–184.

Takeda, K., Cowan, A., and Fong, G.H. (2007). Essential role for prolyl hydroxylase domain protein 2 in oxygen homeostasis of the adult vascular system. Circulation *116*, 774–781.

Takeda, K., Aguila, H.L., Parikh, N.S., Li, X., Lamothe, K., Duan, L.J., Takeda, H., Lee, F.S., and Fong, G.H. (2008). Regulation of adult erythropoiesis by prolyl hydroxylase domain proteins. Blood *111*, 3229–3235.

Thurston, G., Noguera-Troise, I., and Yancopoulos, G.D. (2007). The Delta paradox: DLL4 blockade leads to more tumour vessels but less tumour growth. Nat. Rev. Cancer *7*, 327–331.

Winkler, F., Kozin, S.V., Tong, R.T., Chae, S.S., Booth, M.F., Garkavtsev, I., Xu, L., Hicklin, D.J., Fukumura, D., di Tomaso, E., et al. (2004). Kinetics of vascular normalization by VEGFR2 blockade governs brain tumor response to radiation: role of oxygenation, angiopoietin-1, and matrix metalloproteinases. Cancer Cell *6*, 553–563.

Wu, S., Nishiyama, N., Kano, M.R., Morishita, Y., Miyazono, K., Itaka, K., Chung, U.I., and Kataoka, K. (2008). Enhancement of angiogenesis through stabilization of hypoxia-inducible factor-1 by silencing prolyl hydroxylase domain-2 gene. Mol. Ther. *16*, 1227–1234.

Yamashita, T., Ohneda, K., Nagano, M., Miyoshi, C., Kaneko, N., Miwa, Y., Yamamoto, M., Ohneda, O., and Fujii-Kuriyama, Y. (2008). Hypoxia-inducible transcription factor-2alpha in endothelial cells regulates tumor neovascularization through activation of ephrin A1. J. Biol. Chem. *283*, 18926–18936.